

## Nonlocal drag thermoelectricity generated by ferroelectric van der Waals heterostructures

Ping Tang <sup>1</sup>, Ken-ichi Uchida <sup>2,3</sup> and Gerrit E. W. Bauer <sup>1,3,4,5,6</sup>

<sup>1</sup>WPI-AIMR, Tohoku University, 2-1-1 Katahira, Sendai 980-8577, Japan

<sup>2</sup>National Institute for Materials Science, Tsukuba 305-0047, Japan

<sup>3</sup>Institute for Materials Research, Tohoku University, 2-1-1 Katahira, Sendai 980-8577, Japan

<sup>4</sup>Center for Spintronics Research Network, Tohoku University, Sendai 980-8577, Japan

<sup>5</sup>Zernike Institute for Advanced Materials, University of Groningen, 9747 AG Groningen, Netherlands

<sup>6</sup>Kavli Institute for Theoretical Sciences, University of the Chinese Academy of Sciences, Beijing 10090, China



(Received 1 July 2022; revised 19 February 2023; accepted 9 March 2023; published 21 March 2023)

The “ferron” excitations of the electric-dipolar order carry energy as well as electric dipoles. Here, we predict a nonlocal ferron-drag effect in a ferroelectric on top of a metallic film: An electric current in the conductor generates a heat current in the ferroelectric by long-range charge-dipole interactions. The nonlocal Peltier and its reciprocal Seebeck effect can be controlled by electric gates and detected thermographically. We predict large effects for van der Waals ferroelectric films on graphene.

DOI: [10.1103/PhysRevB.107.L121406](https://doi.org/10.1103/PhysRevB.107.L121406)

The electron-electron interaction between closely spaced two-dimensional electron gases (2DEGs) gives rise to *non-local* Coulomb drag effects [1–3], in which a current in an active layer induces a voltage over the passive one. The concept of Coulomb drag has been extended to other systems and interactions. A *local* drag effect by the electron-phonon interaction contributes to the thermopower in bulk conductors [4–7] and also a nonlocal drag effect can be mediated by phonons in the spacer between the 2DEGs [8–10]. In ferromagnetic metals, magnons, the quasiparticle excitations of local magnetization, transfer their momenta to conduction electrons by the exchange interaction. This local magnon drag effect enhances the Seebeck and Peltier coefficients [11–16]. The voltage in one layer induced by a current in the other in a heavy metal/ferromagnetic insulator/heavy metal stack is a nonlocal drag effect caused by the spin Hall effect [17–19]. Theory predicts that magnons in magnetic films separated by a vacuum barrier experience a nonlocal drag effect by the magnetodipolar interaction [20]. The magnetodipolar interaction can also mediate an energy transfer through an air gap [21], but a nonlocal magnon drag effect has not yet been observed.

Ferroelectrics exhibit an electrically switchable spontaneous polarization that orders below a Curie temperature. Recently, we introduced “ferrons,” the bosonic excitations of ferroelectric order that carry elementary electric dipoles in the presence of transverse [22,23] or longitudinal fluctuations [24]. Ferrons are the anharmonic symmetry-restoring fluctuations on top of the symmetry-broken ground state. So while in displacive ferroelectrics [25,26] ferrons are also phonons, the phonons in normal dielectrics are not ferrons. A direct experimental observation of the predicted polarization and heat transport phenomena, e.g., by the transient Peltier effect [22] and associated stray fields [23], may not be so simple, however.

Here, we pursue ideas to simplify the detection of ferronic effects via nonlocal thermoelectric drag effects in bilayers of a ferroelectric and a metal, which opens unconventional strate-

gies for heat-to-electricity conversion. We consider a film of a perpendicularly polarized ferroelectric insulator on top of an extended metallic sheet that experiences a “ferron drag” in the form of a nonlocal Peltier effect, i.e., a heat current in the ferroelectric generated by an electric current in the metal film (see Fig. 1). We assume that the electric dipoles are all located in a common plane and that the electrons in the metal move in a parallel plane. This two-dimensional (2D) assumption is valid when the two films are separated by a distance  $d$  much larger than their thickness, but certainly appropriate when the conductor is, e.g., graphene and the ferroelectric a van der Waals mono- or bilayer [27–34].

The linear response relations of transport or Ohm’s law in our bilayer (in the  $x$  direction) connect four driving forces, i.e., an in-plane electric field  $E_M$  in the metal, a gradient of an out-of-plane electric field  $\partial E_{FE}$  in the ferroelectric, and independent temperature gradients in the two films, with the charge current  $j_c$  in the metal, polarization current  $j_p$  in the ferroelectric, and the heat currents  $j_q^{(M)}$  and  $j_q^{(FE)}$ ,

$$\begin{pmatrix} -j_c \\ j_q^{(M)} \\ -j_p \\ j_q^{(FE)} \end{pmatrix} = \begin{pmatrix} L_{11} & L_{12} & L_{13} & L_{14} \\ L_{12} & L_{22} & L_{23} & L_{24} \\ L_{13} & L_{23} & L_{33} & L_{34} \\ L_{14} & L_{24} & L_{34} & L_{44} \end{pmatrix} \begin{pmatrix} -E_M \\ -\partial \ln T_M \\ \partial E_{FE} \\ -\partial \ln T_{FE} \end{pmatrix}, \quad (1)$$

where we already inserted the Onsager-Kelvin relation  $L_{ij} = L_{ji}$  between the off-diagonal transport coefficients. We focus here on the steady state with finite  $E_M$  that induces polarization and heat currents in the ferroelectric. In the following, we disregard small thermoelectric effects in the metal and thermal leakage between the films. This assumption holds for efficient interlayer thermal isolation and a metallic sheet with high thermal conductivity. The task then reduces to the calculation of the polarization drag  $\vartheta_D \equiv L_{13}/L_{11}$  as well as

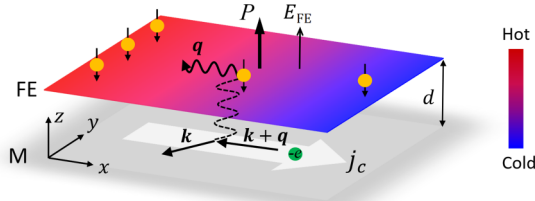


FIG. 1. A schematic of the nonlocal ferron-drag Peltier effect between an extended metallic (M) and a perpendicularly polarized and electrically insulating ferroelectric (FE) film. A charge current ( $j_c$ ) in the active M sheet transfers its linear momentum to the ferrons in the FE by the electrostatic interaction, leading to heat accumulations at the FE edges. The orange balls represent the ferrons, while the small black arrows are the ferron dipoles that oppose the ferroelectric order and can couple with an out-of-plane electric field ( $E_{FE}$ ).

the thermoelectric effects summarized by

$$\begin{pmatrix} -j_c \\ j_q^{(FE)} \end{pmatrix} = \begin{pmatrix} L_{11} & L_{14} \\ L_{14} & L_{44} \end{pmatrix} \begin{pmatrix} -E_M \\ -\partial \ln T_{FE} \end{pmatrix}, \quad (2)$$

in which we identify the nonlocal Peltier coefficient  $\pi_D = L_{14}/L_{11}$  and thermopower  $s_D = \pi_D/T_{FE}$ . The electrical conductivity  $\sigma = L_{11}$  is also affected by the equilibrium fluctuations of the nearby ferroelectric.

The conduction electrons in the metallic layer interact with the electric polarization  $\mathbf{P}(\mathbf{r}) = P(\mathbf{r}_{\parallel})\delta(z-d)\hat{\mathbf{z}}$  of the ferroelectric at  $z = d$  by the electrostatic energy

$$\mathcal{H}_{\text{int}} = - \int \mathbf{E}_{\text{el}}(\mathbf{r}) \cdot \mathbf{P}(\mathbf{r}) d\mathbf{r}, \quad (3)$$

where

$$\mathbf{E}_{\text{el}}(\mathbf{r}) = - \frac{e}{4\pi\epsilon_r\epsilon_0} \int d\mathbf{r}' \frac{n(\mathbf{r}')}{|\mathbf{r} - \mathbf{r}'|^3} (\mathbf{r} - \mathbf{r}') \quad (4)$$

is the Hartree field of the electrons,  $-e$  the electron charge,  $n(\mathbf{r}) = n(\mathbf{r}_{\parallel})\delta(z)$  the electron density in the metal at  $z = 0$ , and  $\epsilon_r$  the relative permittivity of the separating barrier. Substituting Eq. (4) leads to

$$\mathcal{H}_{\text{int}} = \frac{ed}{4\pi\epsilon_r\epsilon_0} \iint d\mathbf{r}_{\parallel} d\mathbf{r}'_{\parallel} \frac{P(\mathbf{r}_{\parallel})n(\mathbf{r}'_{\parallel})}{[(\mathbf{r}_{\parallel} - \mathbf{r}'_{\parallel})^2 + d^2]^{3/2}}, \quad (5)$$

where  $P(\mathbf{r}_{\parallel})$  and  $n(\mathbf{r}_{\parallel})$  represent the 2D polarization and electron density in units of C/m and  $\text{m}^{-2}$ , respectively.

We model the ferroelectric by the Landau-Ginzburg-Devonshire free energy [35,36]

$$F = \left( \frac{g}{2} (\nabla P)^2 + \frac{\alpha}{2} P^2 + \frac{\beta}{4} P^4 + \frac{\lambda}{6} P^6 - E_{FE} P \right), \quad (6)$$

where  $\alpha = \alpha_0(T - T_c)$ ,  $\beta$  and  $\lambda > 0$  are the Landau coefficients,  $T_c$  the Curie-Weiss temperature,  $g > 0$  the Ginzburg parameter accounting for the energy cost of an inhomogeneous polarization, and  $E_{FE}$  is an out-of-plane electric field acting on the ferroelectric order. The phase transition for  $\beta < 0$  ( $\beta > 0$ ) is first (second) order. A uniform spontaneous polarization  $P_0$  minimizes  $F$  by  $\alpha P_0 + \beta P_0^3 + \lambda P_0^5 = E_{FE}$ , which gives  $P_0^2 = [-\beta + (\beta^2 - 4\alpha\lambda)^{1/2}]/(2\lambda)$  when  $E_{FE} = 0$ . The

nonlinear static dielectric susceptibility with the field reads

$$\chi(E_{FE}) = \frac{\partial P_0(E_{FE})}{\partial E_{FE}} = \frac{1}{\alpha + 3\beta P_0^2(E_{FE}) + 5\lambda P_0^4(E_{FE})}. \quad (7)$$

Small fluctuations  $\delta P(\mathbf{r}_{\parallel}, t) = P(\mathbf{r}_{\parallel}, t) - P_0$  can be quantized as [24]

$$\delta P(\mathbf{r}_{\parallel}, t) = \sqrt{\frac{\hbar}{2m_p A}} \sum_{\mathbf{q}} \frac{\hat{a}_{\mathbf{q}} e^{i\mathbf{q}\cdot\mathbf{r}_{\parallel}}}{\sqrt{\omega_{\mathbf{q}}}} + \text{H.c.}, \quad (8)$$

where  $m_p$  is the polarization inertia that depends on the ionic masses  $M_i$  and Born effective charges  $Q_i$  in the unit cell of area  $A_0$  as  $m_p = A_0(\sum_i Q_i^2/M_i)^{-1}$  [37],  $A$  the area of the ferroelectric sheet (assumed to be the same as the metal), and  $\hat{a}_{\mathbf{q}}$  ( $\hat{a}_{\mathbf{q}}^\dagger$ ) the annihilation (creation) operator of ferrons with the dispersion relation

$$\omega_{\mathbf{q}} = \left( \frac{gq^2 + \chi(E_{FE})^{-1}}{m_p} \right)^{1/2}. \quad (9)$$

The electric dipole carried by a single ferron is then identified as [24]

$$\delta p_{\mathbf{q}} = - \frac{\partial \hbar \omega_{\mathbf{q}}}{\partial E_{FE}} = \frac{\hbar}{2m_p \omega_{\mathbf{q}}} \frac{\partial \ln \chi}{\partial P_0} < 0, \quad (10)$$

where the negative sign indicates its opposite direction to the ferroelectric order.

In 2D momentum space Eq. (5) now reads

$$\mathcal{H}_{\text{int}} = \frac{e}{2\epsilon_r\epsilon_0 A} \sum_{\mathbf{q}} e^{-dq} n(\mathbf{q}) \int d\mathbf{r}_{\parallel} \delta P(\mathbf{r}_{\parallel}) e^{i\mathbf{q}\cdot\mathbf{r}_{\parallel}}, \quad (11)$$

where we dropped a constant energy shift related to  $P_0$  and  $n(\mathbf{q}) = \sum_{\mathbf{k}\nu\nu'} F_{\mathbf{k}\nu}^\dagger F_{(\mathbf{k}+\mathbf{q})\nu'} \hat{c}_{\mathbf{k}\nu}^\dagger \hat{c}_{(\mathbf{k}+\mathbf{q})\nu'}$  is the Fourier component of the 2D electron density in terms of the field operators  $\hat{c}_{\mathbf{k}\nu}^\dagger$  and  $\hat{c}_{\mathbf{k}\nu}$  with momentum  $\mathbf{k}$ , band index  $\nu$ , and the corresponding spinor wave functions  $F_{\mathbf{k}\nu}$ .  $F_{\mathbf{k}\nu}^\dagger F_{\mathbf{k}\nu} = (e^{i(\theta_{\mathbf{k}'} - \theta_{\mathbf{k}})} + \nu\nu')/2$  ( $=\delta_{\nu,\nu'}$ ) for graphene (normal metals), where  $\tan \theta_{\mathbf{k}} = k_y/k_x$  and  $\nu = +1$  and  $\nu = -1$  indicate the conduction and valence bands, respectively [38,39]. Substituting Eq. (8) yields

$$\mathcal{H}_{\text{int}} = \sum_{\mathbf{k}\mathbf{q}\nu\nu'} V_{\mathbf{k}\mathbf{q}}(\nu', \nu) \hat{c}_{(\mathbf{k}+\mathbf{q})\nu'}^\dagger \hat{c}_{\mathbf{k}\nu} \hat{a}_{\mathbf{q}} + \text{H.c.}, \quad (12)$$

where

$$V_{\mathbf{k}\mathbf{q}}(\nu', \nu) = \frac{e}{2\epsilon_r\epsilon_0} \sqrt{\frac{\hbar}{2m_p A}} \frac{e^{-dq}}{\sqrt{\omega_{\mathbf{q}}}} F_{(\mathbf{k}+\mathbf{q})\nu'}^\dagger F_{\mathbf{k}\nu} \quad (13)$$

is the bare inelastic scattering amplitude of the electrons.

The screening by the conduction electrons and electric dipoles is a many-body problem in which  $V_{\mathbf{k}\mathbf{q}}(\nu', \nu) \rightarrow V_{\mathbf{k}\mathbf{q}}(\nu', \nu)/\epsilon(q, \omega)$  and  $\epsilon(q, \omega)$  is the dielectric function. At sufficiently high conduction electron densities, the ferron energies are small compared to the Fermi energy and we may adopt static screening  $\omega \rightarrow 0$ . For  $q < 1/(2d) \lesssim 2k_F$ , where  $k_F$  is the Fermi wave vector, it is sufficient to adopt the Thomas-Fermi screening approximation [38–43], i.e.,

$$V_{\mathbf{k}\mathbf{q}}(\nu', \nu) \rightarrow U_{\mathbf{k}\mathbf{q}}(\nu', \nu) = \frac{V_{\mathbf{k}\mathbf{q}}(\nu', \nu)}{1 + q_{TF}/q}, \quad (14)$$

where  $q_{\text{TF}} = e^2 D_F / (2\epsilon_r \epsilon_0)$  is the 2D Thomas-Fermi wave vector in terms of the density of state  $D_F$  at Fermi level. The screening by the ferroelectric dipoles is negligibly small compared to that of the free electrons when the ferroelectric sheet is sufficiently thin. The screening then does not depend on  $d$ .

We consider now the effect of a charge current  $j_c$  driven by an electric field ( $E_M$ ) along the  $x$  direction in the metallic sheet that deforms the electron distribution function  $f_{\mathbf{k}v}$  from the Fermi-Dirac form  $f_{\mathbf{k}v}^{(0)} = \{\exp[(\epsilon_{\mathbf{k}v} - \epsilon_F)/k_B T] + 1\}^{-1}$  in momentum space, where  $\epsilon_{\mathbf{k}v}$  is the electronic band structure,  $\epsilon_F$  the Fermi energy,  $T$  the temperature, and  $k_B$  Boltzmann's constant. Within relaxation time approximation the linearized Boltzmann equation in the metal reads

$$f_{\mathbf{k}v} = f_{\mathbf{k}v}^{(0)} + e\tau_e v_{\mathbf{k}v}^{(x)} E_M \frac{\partial f_{\mathbf{k}v}^{(0)}}{\partial \epsilon_{\mathbf{k}v}}, \quad (15)$$

where  $\tau_e$  is the relaxation time and  $v_{\mathbf{k}v}^{(x)} = \partial \epsilon_{\mathbf{k}v} / \partial \hbar k_x$  the group velocities in the transport ( $x$ ) direction, with  $v_{\mathbf{k}v}^{(x)} \rightarrow \hbar k_x / m_e$  ( $v_F k_x / |\mathbf{k}|$ ) for a free-electron gas with effective mass  $m_e$  (or a Dirac cone of graphene with Fermi velocity  $v_F$ ). The associated electric current density reads  $j_c = \sigma E_M$ , where

$$\sigma = \frac{e^2 \tau_e \delta}{A} \sum_{\mathbf{k}} (v_{\mathbf{k}v}^{(x)})^2 \left( -\frac{\partial f_{\mathbf{k}v}^{(0)}}{\partial \epsilon_{\mathbf{k}v}} \right) \quad (16)$$

is the electrical conductivity and  $\delta$  includes the spin and valley degeneracies.

In the Supplemental Material A [44] we derive a ferron-electron scattering contribution that drastically reduces the  $\tau_e$  at the Curie temperature of the ferroelectric. The observation of the predicted critical enhancement of the scattering rate would provide a proof of ferron excitations independent of the thermoelectric effects discussed in the following.

The bosonic ferron distribution function  $N_{\mathbf{q}}$  in the ferroelectric is governed by another linearized Boltzmann equation [24,45]. Far from the edges and in the absence of temperature or effective field gradients, the steady state distribution reads

$$N_{\mathbf{q}} = N_{\mathbf{q}}^{(0)} + \tau_f \frac{\partial N_{\mathbf{q}}}{\partial t} \Big|_{\text{int}}, \quad (17)$$

where  $N_{\mathbf{q}}^{(0)} = [\exp(\hbar\omega_{\mathbf{q}}/k_B T) - 1]^{-1}$  is the equilibrium Planck distribution, and  $\tau_f$  the ferron relaxation time. The new ingredient is the collision integral  $\partial N_{\mathbf{q}} / \partial t|_{\text{int}}$ , which by the current in the metal and via the interlayer interaction  $U_{\mathbf{q}}$  renders  $N_{\mathbf{q}} \neq N_{-\mathbf{q}}$ . The electrons scatter from occupied to empty states, creating and annihilating a ferron in the process. According to Fermi's golden rule,

$$\begin{aligned} \frac{\partial N_{\mathbf{q}}}{\partial t} \Big|_{\text{int}} &= \frac{2\pi\delta}{\hbar} \sum_{\mathbf{k}} |U_{\mathbf{k}\mathbf{q}}|^2 [(1 + N_{\mathbf{q}})f_{(\mathbf{k}+\mathbf{q})v}(1 - f_{\mathbf{k}v}) \\ &\quad - N_{\mathbf{q}}f_{\mathbf{k}v}(1 - f_{(\mathbf{k}+\mathbf{q})v})] \delta(\epsilon_{\mathbf{k}v} - \epsilon_{(\mathbf{k}+\mathbf{q})v} + \hbar\omega_{\mathbf{q}}), \end{aligned} \quad (18)$$

while energy and momentum are conserved. Here, insignificant interband processes ( $v \neq v'$ ) have been discarded. To leading order, we may replace  $N_{\mathbf{q}}$  on the right-hand side of Eq. (18) with  $N_{\mathbf{q}}^{(0)}$  and substitute the distribution function of

the field-biased conductor Eq. (15):

$$\begin{aligned} N_{\mathbf{q}} &= N_{\mathbf{q}}^{(0)} + \frac{2\pi\delta\tau_f}{\hbar} \frac{\partial N_{\mathbf{q}}^{(0)}}{\partial \hbar\omega_{\mathbf{q}}} \sum_{\mathbf{k}} |U_{\mathbf{k}\mathbf{q}}|^2 (f_{(\mathbf{k}+\mathbf{q})v}^{(0)} - f_{\mathbf{k}v}^{(0)}) \\ &\quad \times e\tau_e E_M (v_{\mathbf{k}+\mathbf{q}}^{(x)} - v_{\mathbf{k}}^{(x)}) \delta(\epsilon_{\mathbf{k}v} - \epsilon_{(\mathbf{k}+\mathbf{q})v} + \hbar\omega_{\mathbf{q}}). \end{aligned} \quad (19)$$

We can now derive the nonlocal Peltier  $\pi_D = -j_q^{(\text{FE})}/j_c$  and polarization drag  $\vartheta_D = j_p/j_c$  coefficients by evaluating the heat and polarization currents for the deformed ferron distribution functions by  $j_q^{(\text{FE})} = A^{-1} \sum_{\mathbf{q}} u_{\mathbf{q}}^{(x)} N_{\mathbf{q}} \hbar\omega_{\mathbf{q}}$  and  $j_p = A^{-1} \sum_{\mathbf{q}} u_{\mathbf{q}}^{(x)} N_{\mathbf{q}} \delta p_{\mathbf{q}}$ , respectively, where  $u_{\mathbf{q}}^{(x)} = \partial\omega_{\mathbf{q}}/\partial q_x$  is the ferron group velocity along the  $x$  direction:

$$\begin{aligned} \pi_D &= \frac{2\pi e\tau_f\tau_e\delta}{\sigma\hbar A} \sum_{\mathbf{k}\mathbf{q}} \hbar\omega_{\mathbf{q}} u_{\mathbf{q}}^{(x)} (v_{\mathbf{k}+\mathbf{q}}^{(x)} - v_{\mathbf{k}}^{(x)}) \frac{\partial N_{\mathbf{q}}^{(0)}}{\partial \hbar\omega_{\mathbf{q}}} |U_{\mathbf{k}\mathbf{q}}|^2 \\ &\quad \times (f_{\mathbf{k}+\mathbf{q}v}^{(0)} - f_{\mathbf{k}v}^{(0)}) \delta(\epsilon_{\mathbf{k}v} - \epsilon_{(\mathbf{k}+\mathbf{q})v} + \hbar\omega_{\mathbf{q}}), \end{aligned} \quad (20)$$

$$\begin{aligned} \vartheta_D &= \frac{2\pi e\tau_f\tau_e\delta}{\sigma\hbar A} \sum_{\mathbf{k}\mathbf{q}} \delta p_{\mathbf{q}} u_{\mathbf{q}}^{(x)} (v_{\mathbf{k}+\mathbf{q}}^{(x)} - v_{\mathbf{k}}^{(x)}) \frac{\partial N_{\mathbf{q}}^{(0)}}{\partial \hbar\omega_{\mathbf{q}}} |U_{\mathbf{k}\mathbf{q}}|^2 \\ &\quad \times (f_{\mathbf{k}+\mathbf{q}v}^{(0)} - f_{\mathbf{k}v}^{(0)}) \delta(\epsilon_{\mathbf{k}v} - \epsilon_{(\mathbf{k}+\mathbf{q})v} + \hbar\omega_{\mathbf{q}}). \end{aligned} \quad (21)$$

We proceed by adopting the quasielastic approximation, i.e.,  $\delta(\epsilon_{\mathbf{k}v} - \epsilon_{(\mathbf{k}+\mathbf{q})v} + \hbar\omega_{\mathbf{q}}) \approx \delta(\epsilon_{\mathbf{k}v} - \epsilon_{(\mathbf{k}+\mathbf{q})v})$ , assuming that the Fermi energy is much larger than that of the ferrons ( $\lesssim 10$  meV) [24]. This is the case in graphene with homogeneous electron densities  $n_0 > 10^{12}$  cm $^{-2}$  and Fermi energies  $\epsilon_F > 0.11$  eV [43]. At  $k_B T \ll \epsilon_F$ ,  $f_{\mathbf{k}v} - f_{(\mathbf{k}+\mathbf{q})v} \approx \hbar\omega_{\mathbf{q}} \delta(\epsilon_{\mathbf{k}v} - \epsilon_F)$ , and we find

$$\begin{aligned} \pi_D &\simeq \frac{e\tau_f g \hbar^3 D_F^2}{32\delta m_p^2 \epsilon_0^2 n_0 k_F k_B T} \int_0^{2k_F} \frac{\cos^2(\theta/2) q^2 dq}{\sqrt{1 - (q/2k_F)^2}} \\ &\quad \times \frac{e^{-2dq}}{(1 + q_{\text{TF}}/q)^2} \text{csch}^2\left(\frac{\hbar\omega_{\mathbf{q}}}{2k_B T}\right). \end{aligned} \quad (22)$$

In contrast to the free-electron gas there is a factor  $\cos^2(\theta/2)$  that arises from the overlap  $|F_{(\mathbf{k}+\mathbf{q})v}^\dagger F_{\mathbf{k}v}|^2$ , where  $\theta$  is the scattering angle determined by  $q = 2k_F \sin(\theta/2)$ . A similar expression can be derived for  $\vartheta_D$  by replacing  $\hbar\omega_{\mathbf{q}}$  with  $\delta p_{\mathbf{q}}$ .

The spatial separation limits the momentum transfer exponentially via the factor  $\exp(-2dq)$  to  $q < 1/(2d)$ . At large distances with  $k_F d \gg 1$ ,  $q_{\text{TF}} d \gg 1$ , and  $d \gg l \equiv \sqrt{g\chi}$ , only the ferrons located near the center of Brillouin zone contribute and

$$\begin{aligned} \pi_D &\approx \frac{3\pi}{8\delta^2} \frac{\tau_f \omega_0}{(k_F d)^3} \left(\frac{l}{d}\right)^2 \left(\frac{\hbar^2}{e^3 m_p}\right) \xi_0 \text{csch}^2\left(\frac{\xi_0}{2}\right) \\ &\simeq \frac{3\pi}{2\delta^2} \frac{\tau_f \omega_0}{(k_F d)^3} \left(\frac{l}{d}\right)^2 \left(\frac{\hbar^2}{e^3 m_p}\right) \begin{cases} \xi_0 e^{-\xi_0} & \text{for } \xi_0 \gg 1, \\ \xi_0^{-1} & \text{for } \xi_0 \ll 1, \end{cases} \\ \vartheta_D &\approx \frac{\pi_D}{2} \frac{\partial \chi}{\partial P_0}, \end{aligned} \quad (23)$$

where  $\xi_0 = \hbar\omega_0/k_B T$  and  $\omega_0 = (\chi m_p)^{-1/2}$  the ferron gap.  $l \equiv \sqrt{g\chi}$  is the coherence length of the ferroelectric order, a measure of the ferroelectric domain wall width [46,47]. Since magnetic domain wall widths that scale as  $\sim \sqrt{J/K}$ , where  $J$  is the exchange interaction and  $K$  is the anisotropy that governs

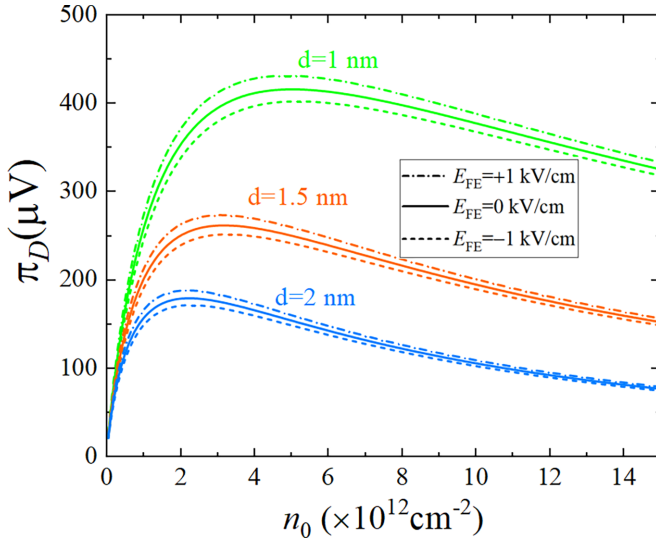


FIG. 2. The nonlocal ferron-drag Peltier coefficient ( $\pi_D$ ) as a function of the electron concentration ( $n_0$ ) in graphene for various interlayer distances ( $d$ ). The  $\pi_D$  exhibit an asymmetric dependence on the relative direction of an external field ( $E_{FE}$ ) to the ferroelectric order.

the magnon gap, and  $\chi^{-1}$  plays the role of the anisotropy by stiffening the ferroelectric order.

The  $T/d^5$  scaling relation at large distances and elevated temperatures for the drag efficiency differs from that of the Coulomb drag effect between two metallic sheets ( $\sim T^2/d^4$ ) [1,2]. We can trace the difference to the faster decay of electron-dipole interactions ( $\sim r^{-2}$ ) compared to those between charges ( $\sim r^{-1}$ ) as a function of distance while the Planck distribution of the ferrons compared to the Fermi distribution of electrons leads to an increased phase space for scatterings at low temperatures ( $k_B T \ll \varepsilon_F$ ).

For a numerical estimate, we consider here a bilayer composed of graphene and a van der Waals ferroelectric monolayer and separated by an inert hexagonal boron nitride (hBN) layer with (out-of-plane)  $\varepsilon_r = 3.76$  [48]. In graphene  $\varepsilon_{\mathbf{k}v} = v\hbar v_F |\mathbf{k}|$  with  $v_F = 10^8$  cm/s,  $D_F = 2\varepsilon_F/(\pi\hbar^2 v_F^2)$ ,  $\delta = 4$ , and  $k_F = (4\pi n_0/\delta)^{1/2}$  [43]. Since we could not find the model parameters of a 2D ferroelectric with out-of-plane polarization in the literature, we adopt numbers close to the well-documented in-plane ferroelectric monolayer SnSe [49]:  $\tau_f = 1$  ps,  $T_c = 326$  K,  $\alpha_0 = 1.54 \times 10^3$  V K $^{-1}$ /pC,  $\beta = 1.48 \times 10^5$  V cm $^2$ /pC $^3$ ,  $\lambda = 2.75 \times 10^4$  V cm $^4$ /pC $^5$ ,  $g = 0.33$  V m $^2$ /C, and  $m_p = 10^{-8}$  V s $^2$ /C. Figure 2 shows the ferron-drag Peltier coefficient as a function of graphene excess electron density ( $n_0$ ) for various interlayer distances  $d$  at room temperature.  $\pi_D$  has a maximum at an optimal  $n_0$  that decreases with  $d$  because a larger  $n_0$  increases the electron-ferron scattering for small  $n_0$  while the increased screening wins at larger densities, which is easier for larger  $d$ .  $\pi_D$  depends not only on the strength, but also on the direction of an external electric field (below the coercive field), i.e.,  $\pi_D$  is reduced (enhanced) by the positive (negative) field along the ferroelectric order, because of the fact that the ferrons carry nonzero electric dipoles.

The drag effect results in heat and polarization accumulations in the ferroelectric (see Fig. 1). Assuming that both films are thermally isolated, a temperature gradient  $T_{FE}(x) = T_0 + \partial T_{FE}(x - L/2)$  emerges in a ferroelectric with length  $L$ , where  $T_0$  is the ambient temperature. The open circuit condition for the heat current, i.e.,  $j_q^{(FE)} = -\pi_D j_c - \kappa_{FE} \partial T_{FE} = 0$ , leads to  $\partial T_{FE} = (-\pi_D/\kappa_{FE}) j_c$ , where  $\kappa_{FE}$  is the 2D thermal conductivity of the ferroelectric sheet (in units of W/K). The polarization accumulation  $\Delta P(x)$  vanishes except for the neighborhood of the edges on the scale of the polarization relaxation length [22].

With  $d = 1$  nm,  $n_0 = 10^{13}$  cm $^{-2}$ , we have  $\pi_D = 367$   $\mu$ V at the room temperature. The maximum current density in graphene is limited by self-heating to  $\sim 30$  A/cm [50], but even for  $j_c = 3.4 \times 10^{-2}$  A/cm (or a bulk current density  $j_c^{(b)} = 10^6$  A/cm $^2$ ) this modest Peltier coefficient generates a large temperature gradient  $\partial T_{FE} = 5$  K/ $\mu$ m for  $\kappa_{FE} = 2.5 \times 10^{-10}$  W/K (or bulk  $\kappa_{FE}^{(b)} = 0.5$  W/Km for a monolayer thickness of 5  $\text{\AA}$  [51]) because of the simultaneous low thermal conductivity of the ferroelectric and high available current density in graphene. This should be easily observable close to the edges, even when some heat current leaks from the ferroelectric into the graphene. Inversely, a temperature gradient in the ferroelectric generates a charge current in graphene, i.e., a nonlocal ferron-drag thermopower.  $s_D = \pi_D/T_0 = 1.23$   $\mu$ V/K at  $T_0 = 298$  K. However, this number is at least an order of magnitude smaller than that of a single graphene [52,53].

For sufficient thermal isolation between the ferroelectric and graphene layers the figure of merit of the ferron-drag thermoelectric device can be defined and estimated as

$$(ZT)_D = \frac{\sigma s_D^2 T_0}{\kappa_{FE}} = 2.6 \times 10^{-3}, \quad (24)$$

where  $\sigma = 1.38 \times 10^{-3}$  S is the electrical conductivity with the nearby ferroelectric at  $n_0 = 10^{13}$  cm $^{-2}$  [44]. This  $(ZT)_D$  is comparable to that of graphene [54] but it may be engineered to become larger by, e.g., optimizing the electron density of graphene as shown in Fig. 2 or stacking  $m$  ferroelectric monolayers with  $(ZT)_D \propto m$  as long as all of them stay in the range of the dipolar interaction and the ferroelectric maintains its two-dimensional properties. The predicted substantial figure of merit (FOM) in spite of the small  $s_D$  relies on beating the Wiedemann-Franz law that hinders conventional thermoelectric devices: The small heat conductivity in the ferroelectric does not depend on the electric conductivity in the conductor, which is large in graphene in spite of the additional ferron scattering [44].

According to Supplemental Material B [44] the current drag is not specific for ferrons: The expressions are identical for in-plane longitudinal and out-of-plane polarized optical phonons, except for the difference in the frequency dispersions and other relevant parameters. We therefore encourage the search for thermoelectric effects in any highly polarizable insulator. The attraction of using ferroelectrics is strong dependence and control of larger effects by temperature and applied electric field as well as nonvolatile switching

of the ferroelectric order. The critical enhancement of the electrical resistance at the Curie temperature is also unique for ferroelectrics.

*Conclusion.* We predict significant nonlocal ferron-drag thermoelectric effects in bilayers of ferroelectric insulators and conductors that are separated by a small distance  $d$ . A remote gate-field-controlled Peltier effect can be detected by standard thermography and would prove the existence of the ferron quasiparticles in ferroelectrics. The results can be readily extended to the limit  $d = 0$  corresponding to van der Waals conducting ferroelectrics, known as ferroelectric metals, in which electric polarization and mobile electrons coexist [55], and the ferroelectrics with in-plane spontaneous polarization. In the dipole approximation of the ferroelectric charge dy-

namics, the mobile electrons cannot screen the perpendicular ferroelectric order nor couple to the longitudinal ferrons. We may expect a strong coupling to the transverse ferrons, however, with associated interesting thermoelectric phenomena presently under investigation. Our work opens strategies for the design of thermoelectric devices that are not bound by the Wiedemann-Franz law.

*Acknowledgments.* We acknowledge helpful discussions with Ryo Iguchi. JSPS KAKENHI Grant No. 19H00645 supported P.T. and G.B. and Grant No. 22H04965 supported G.B. and K.U. K.U. also acknowledges support by JSPS KAKENHI Grant No. 20H02609 and JST CREST “Creation of Innovative Core Technologies for Nano-enabled Thermal Management” Grant No. JPMJCR1711.

- 
- [1] T. J. Gramila, J. P. Eisenstein, A. H. MacDonald, L. N. Pfeiffer, and K. W. West, Mutual Friction between Parallel Two-Dimensional Electron Systems, *Phys. Rev. Lett.* **66**, 1216 (1991).
- [2] A. Jauho and H. Smith, Coulomb drag between parallel two-dimensional electron systems, *Phys. Rev. B* **47**, 4420 (1993).
- [3] B. N. Narozhny and A. Levchenko, Coulomb drag, *Rev. Mod. Phys.* **88**, 025003 (2016).
- [4] M. Bailyn, Phonon-drag part of the thermoelectric power in metals, *Phys. Rev.* **157**, 480 (1967).
- [5] D. Cantrell and P. Butcher, A calculation of the phonon-drag contribution to the thermopower of quasi-2D electrons coupled to 3D phonons, *J. Phys. C* **20**, 1985 (1987).
- [6] S. K. Lyo, Low-temperature phonon-drag thermoelectric power in heterojunctions, *Phys. Rev. B* **38**, 6345(R) (1988).
- [7] J. Vavro, M. C. Llaguno, J. E. Fischer, S. Ramesh, R. K. Saini, L. M. Ericson, V. A. Davis, R. H. Hauge, M. Pasquali, and R. E. Smalley, Thermoelectric Power of  $p$ -Doped Single-Wall Carbon Nanotubes and the Role of Phonon Drag, *Phys. Rev. Lett.* **90**, 065503 (2003).
- [8] H. C. Tso, P. Vasilopoulos, and F. M. Peeters, Direct Coulomb and Phonon-Mediated Coupling Between Spatially Separated Electron Gases, *Phys. Rev. Lett.* **68**, 2516 (1992).
- [9] M. C. Bønsager, K. Flensberg, B. Y. Hu, and A. H. MacDonald, Frictional drag between quantum wells mediated by phonon exchange, *Phys. Rev. B* **57**, 7085 (1998).
- [10] H. Noh, S. Zelakiewicz, T. J. Gramila, L. N. Pfeiffer, and K. W. West, Phonon-mediated drag in double-layer two-dimensional electron systems, *Phys. Rev. B* **59**, 13114 (1999).
- [11] M. Bailyn, Maximum Variational Principle for Conduction Problems in a Magnetic Field, and the Theory of Magnon Drag, *Phys. Rev.* **126**, 2040 (1962).
- [12] F. Blatt, D. Flood, V. Rowe, P. Schroeder, and J. Cox, Magnon-Drag Thermopower in Iron, *Phys. Rev. Lett.* **18**, 395 (1967).
- [13] G. N. Grannemann and L. Berger, Magnon-drag Peltier effect in a Ni-Cu alloy, *Phys. Rev. B* **13**, 2072 (1976).
- [14] M. V. Costache, G. Bridoux, I. Neumann, and S. O. Valenzuela, Magnon-drag thermopile, *Nat. Mater.* **11**, 199 (2012).
- [15] B. Flebus, R. A. Duine, and Y. Tserkovnyak, Landau-Lifshitz theory of the magnon-drag thermopower, *Europhys. Lett.* **115**, 57004 (2016).
- [16] S. J. Watzman, R. A. Duine, Y. Tserkovnyak, S. R. Boona, H. Jin, A. Prakash, Y. Zheng, and J. P. Heremans, Magnon-drag thermopower and Nernst coefficient in Fe, Co, and Ni, *Phys. Rev. B* **94**, 144407 (2016).
- [17] S. S.-L. Zhang and S. Zhang, Magnon Mediated Electric Current Drag Across a Ferromagnetic Insulator Layer, *Phys. Rev. Lett.* **109**, 096603 (2012).
- [18] H. Wu, C. H. Wan, X. Zhang, Z. H. Yuan, Q. T. Zhang, J. Y. Qin, H. X. Wei, X. F. Han, and S. Zhang, Observation of magnon-mediated electric current drag at room temperature, *Phys. Rev. B* **93**, 060403(R) (2016).
- [19] J. Li, Y. Xu, M. Aldosary, C. Tang, Z. Lin, S. Zhang, R. Lake, and J. Shi, Observation of magnon-mediated current drag in Pt/yttrium iron garnet/Pt(Ta) trilayers, *Nat. Commun.* **7**, 10858 (2016).
- [20] T. Liu, G. Vignale, and M. E. Flatté, Nonlocal Drag of Magnons in a Ferromagnetic Bilayer, *Phys. Rev. Lett.* **116**, 237202 (2016).
- [21] Y. Kainuma, R. Iguchi, D. Prananto, V. I. Vasyuchka, B. Hillebrands, T. An, and K. Uchida, Local heat emission due to unidirectional spin-wave heat conveyer effect observed by lock-in thermography, *Appl. Phys. Lett.* **118**, 222404 (2021).
- [22] G. E. W. Bauer, R. Iguchi, and K. Uchida, Theory of Transport in Ferroelectric Capacitors, *Phys. Rev. Lett.* **126**, 187603 (2021).
- [23] P. Tang, R. Iguchi, K. Uchida, and G. E. W. Bauer, Thermoelectric Polarization Transport in Ferroelectric Ballistic Point Contacts, *Phys. Rev. Lett.* **128**, 047601 (2022).
- [24] P. Tang, R. Iguchi, K. Uchida, and G. E. W. Bauer, Excitations of the ferroelectric order, *Phys. Rev. B* **106**, L081105 (2022).
- [25] W. Cochran, Crystal Stability and the Theory of Ferroelectricity, *Phys. Rev. Lett.* **3**, 412 (1959).
- [26] W. Cochran, Crystal stability and the theory of ferroelectricity, *Adv. Phys.* **9**, 387 (1960).
- [27] K. Chang, J. Liu, H. Lin, N. Wang, K. Zhao, A. Zhang, F. Jin, Y. Zhong, X. Hu, W. Duan, Q. Zhang, L. Fu, Q.-K. Xue, X. Chen, and S.-H. Ji, Discovery of robust in-plane ferroelectricity in atomic-thick SnTe, *Science* **353**, 274 (2016).
- [28] F. Liu, L. You, K. L. Seyler, X. Li, P. Yu, J. Lin, X. Wang, J. Zhou, H. Wang, H. He, S. T. Pantelides, W. Zhou, P. Sharma, X. Xu, P. M. Ajayan, J. Wang, and Z. Liu, Room-temperature

- ferroelectricity in CuInP<sub>2</sub>S<sub>2</sub> ultrathin flakes, *Nat. Commun.* **7**, 12357 (2016).
- [29] L. Li and M. Wu, Binary compound bilayer and multilayer with vertical polarizations: Two-dimensional ferroelectrics, multiferroics, and nanogenerators, *ACS Nano* **11**, 6382 (2017).
- [30] Q. Yang, M. Wu, and J. Li, Origin of two-dimensional vertical ferroelectricity in WTe<sub>2</sub> bilayer and multilayer, *J. Phys. Chem. Lett.* **9**, 7160 (2018).
- [31] Z. Fei, W. Zhao, T. A. Palomaki, B. Sun, M. K. Miller, Z. Zhao, J. Yan, X. Xu, and D. H. Cobden, Ferroelectric switching of a two-dimensional metal, *Nature (London)* **560**, 336 (2018).
- [32] S. Yuan, X. Luo, H. L. Chan, C. Xiao, Y. Dai, M. Xie, and J. Hao, Room-temperature ferroelectricity in MoTe<sub>2</sub> down to the atomic monolayer limit, *Nat. Commun.* **10**, 1775 (2019).
- [33] K. Yasuda, X. Wang, K. Watanabe, T. Taniguchi, and P. Jarillo-Herrero, Stacking-engineered ferroelectricity in bilayer boron nitride, *Science* **372**, 1458 (2021).
- [34] X. Wang, K. Yasuda, Y. Zhang, S. Liu, K. Watanabe, T. Taniguchi, J. Hone, L. Fu, and P. Jarillo-Herrero, Interfacial ferroelectricity in rhombohedral-stacked bilayer transition metal dichalcogenides, *Nat. Nanotechnol.* **17**, 367 (2022).
- [35] A. F. Devonshire, Theory of barium titanate: Part I, *London, Edinburgh Dublin Philos. Mag. J. Sci.* **40**, 1040 (1949).
- [36] A. F. Devonshire, Theory of barium titanate: Part II, *London, Edinburgh Dublin Philos. Mag. J. Sci.* **42**, 1065 (1951).
- [37] S. Sivasubramanian, A. Widom, and Y. N. Srivastava, Physical kinetics of ferroelectric hysteresis, *Ferroelectrics* **300**, 43 (2004).
- [38] T. Ando, Screening effect and impurity scattering in monolayer graphene, *J. Phys. Soc. Jpn.* **75**, 074716 (2006).
- [39] E. H. Hwang and S. D. Sarma, Screening-induced temperature-dependent transport in two-dimensional graphene, *Phys. Rev. B* **79**, 165404 (2009).
- [40] F. Stern, Polarizability of a Two-Dimensional Electron Gas, *Phys. Rev. Lett.* **18**, 546 (1967).
- [41] T. Ando, A. B. Fowler, and F. Stern, Electronic properties of two-dimensional systems, *Rev. Mod. Phys.* **54**, 437 (1982).
- [42] E. H. Hwang and S. Das Sarma, Dielectric function, screening, and plasmons in two-dimensional graphene, *Phys. Rev. B* **75**, 205418 (2007).
- [43] S. Das Sarma, S. Adam, E. H. Hwang, and E. Rossi, Electronic transport in two-dimensional graphene, *Rev. Mod. Phys.* **83**, 407 (2011).
- [44] See Supplemental Material at <http://link.aps.org/supplemental/10.1103/PhysRevB.107.L121406> for the influence of ferron-electron scatterings on the electrical conductivity in the metal and the drag effect of in-plane polarization fluctuations (polar optical phonons).
- [45] G. E. W. Bauer, P. Tang, R. Iguchi, and K. Uchida, Magnonics vs ferronics, *J. Magn. Magn. Mater.* **541**, 168468 (2022).
- [46] Y. Ishibashi, Phenomenological theory of domain walls, *Ferroelectrics* **98**, 193 (1989).
- [47] Y. Ishibashi, Structure and physical properties of domain walls, *Ferroelectrics* **104**, 299 (1990).
- [48] A. Laturia, M. L. van de Put, and W. G. Vandenberghe, Dielectric properties of hexagonal boron nitride and transition metal dichalcogenides: From monolayer to bulk, *npj 2D Mater. Appl.* **2**, 6 (2018).
- [49] R. Fei, W. Kang, and L. Yang, Ferroelectricity and Phase Transitions in Monolayer Group-IV Monochalcogenides, *Phys. Rev. Lett.* **117**, 097601 (2016).
- [50] A. D. Liao, J. Z. Wu, X. Wang, K. Tahy, D. Jena, H. Dai, and E. Pop, Thermally Limited Current Carrying Ability of Graphene Nanoribbons, *Phys. Rev. Lett.* **106**, 256801 (2011).
- [51] C. Li, J. Hong, A. May, D. Bansal, S. Chi, T. Hong, G. Ehlers, and O. Delaire, Ultralow thermal conductivity and high thermoelectric figure of merit in SnSe crystals, *Nat. Phys.* **11**, 1063 (2015).
- [52] Y. M. Zuev, W. Chang, and P. Kim, Thermoelectric and Magnetothermoelectric Transport Measurements of Graphene, *Phys. Rev. Lett.* **102**, 096807 (2009).
- [53] P. Wei, W. Bao, Y. Pu, C. N. Lau, and J. Shi, Anomalous Thermoelectric Transport of Dirac Particles in Graphene, *Phys. Rev. Lett.* **102**, 166808 (2009).
- [54] A. H. Reshak, S. A. Khan, and S. Auluck, Thermoelectric properties of a single graphene sheet and its derivatives, *J. Mater. Chem. C* **2**, 2346 (2014).
- [55] W. X. Zhou and A. Ariando, Review on ferroelectric/polar metals, *Jpn. J. Appl. Phys.* **59**, SI0802 (2020).